applied sciences

Article

Bearing Fault Diagnosis Based on Vibration Envelope Spectral Characteristics

Yang Chen *, Qifu Chen and Rui Wang

School of Microelectronics and Control Engineering, Changzhou University, Changzhou 213159, China; s22060858004@smail.cczu.edu.cn (Q.C.); wangrui@cczu.edu.cn (R.W.)
* Correspondence: chenyangcczu@cczu.edu.cn

Abstract: Deep learning methods based on neural network models have been widely applied to bearing fault classification. Although they can achieve high accuracy, they also come with significant complexity. Bearing faults often generate impact vibrations, which produce regular fault characteristic peaks on the envelope spectrum. This paper utilizes the differences in frequency and intensity of the envelope spectrum characteristic peaks under different bearing fault conditions as fault features. By combining these features with the simple and efficient Naive Bayes classifier for fault diagnosis, the algorithm complexity is reduced from the perspective of feature extraction and fault identification. The proposed method was validated using bearing fault data from the Case Western Reserve University (CWRU) dataset and the Machinery Fault Prediction Technology (MFPT) dataset. The results show that the method can classify bearing faults and achieve accurate diagnostic results. The average diagnostic accuracy for the four groups from these two datasets was 99.90% and 99.65%, respectively. The Naive Bayes classification algorithm was compared with classic algorithms in terms of classification accuracy and classification time. Additionally, the algorithm was compared with recent bearing fault diagnosis methods using the CWRU dataset in terms of algorithm complexity. The complexity of the proposed algorithm is only O(N(2280)), which is lower than that of other bearing fault diagnosis methods, where N represents the number of fault samples. This demonstrates that the method significantly reduces algorithm complexity while ensuring accuracy, improving diagnostic efficiency, enhancing the timeliness of real-time industrial bearing fault diagnosis, and reducing hardware setup and operating costs.

Keywords: bearings fault; envelope spectrum; Hilbert demodulation; naive Bayes

check for updates

Academic Editor: Rui Araújo

Received: 23 December 2024
Revised: 2 February 2025
Accepted: 18 February 2025
Published: 19 February 2025

Citation: Chen, Y.; Chen, Q.; Wang, R. Bearing Fault Diagnosis Based on Vibration Envelope Spectral Characteristics. *Appl. Sci.* **2025**, *15*, 2240. https://doi.org/10.3390/app15042240

1. Introduction

The development of rotating mechanical equipment is moving towards refinement and complexity, with increasing demands for reliability. Due to the complexity of its working conditions and harsh operating environment, its parts are prone to damage. Even minor faults during operation can lead to the failure of components or the entire system and, in severe cases, can cause destructive damage and major accidents. Therefore, efficient, fast, and accurate assessment and identification of the health status of rotating mechanical equipment is crucial for improving its safe and reliable operation [1].

Rolling bearings are the core components of rotating machinery, and their reliability in operation is crucial for the accuracy and service life of the entire machine [2]. Bearing failures can lead to abnormal working conditions, resulting in a series of vibration impacts and shock attenuation responses. The collected vibration signals of bearings exhibit a certain degree of non-stationarity and periodic impact characteristics. Therefore, in engineering practice, signal processing methods are often used to identify and extract fault characteristic components from the vibration signals of rolling bearings to achieve condition monitoring and fault diagnosis of the bearings.

In practical applications, bearing fault diagnosis is mainly conducted using vibration signals. The process of rolling bearing fault diagnosis based on vibration signals can be divided into two steps: feature extraction and fault recognition. Since it is challenging to extract features directly from raw signals that can differentiate between different defective states and normal states of bearings, vibration analysis techniques, including time domain analysis, frequency domain analysis, and time–frequency domain analysis, are employed to address this issue [3].

Time domain analysis is based on analyzing the characteristics of a signal over time. We can reveal the signal's dynamic behavior and characteristics by observing features such as the waveform, amplitude, and frequency as the signal changes over time. Frequency-domain analysis transforms a signal into a series of discrete frequency components, making it easy to analyze. The signal is called the signal spectrum after transforming characteristic frequency components for fault analysis. Standard frequency domain analysis methods include peak spectrum analysis [4] and envelope spectrum analysis [5]. Time–frequency domain analysis methods simultaneously study the characteristics of signals in both the time and frequency domains. This enables a more comprehensive understanding of the dynamic properties of the signal and reveals its changing patterns in time and frequency. There are many time–frequency domain analysis methods, such as wavelet analysis [6,7], Wagner–Ville distribution, and variational mode decomposition (VMD) [8,9].

Fault recognition, also known as fault pattern recognition, involves extracting information containing equipment fault characteristics from historical fault data. A fault diagnosis model is established by training on historical feature information using machine learning, deep learning, and other methods. Subsequently, the model identifies and diagnoses equipment by inputting test samples into the trained fault diagnosis model. Commonly used methods include the K-Nearest Neighbor (KNN) [3], random forest (RF) [10], Support Vector Machine (SVM) [11–13], Naive Bayes (NB), convolutional neural networks (CNN) [14], Long Short-Term Memory (LSTM) [15], and recurrent neural networks (RNNs) [16,17].

With the advancement and development of technology, fault diagnosis methods are constantly evolving. Kaya et al. [18] suggested using continuous wavelet transform CWT and convolutional neural networks to predict the bearing fault size diagnosis based on deep transfer learning algorithms (DTL) and time–frequency images. Roy et al. [10] proposed an autocorrelation-assisted feature extraction method, which extracts the top-ranked feature vectors through dimensionality reduction and sends them to a random forest classifier for rolling bearing fault diagnosis. Li et al. [19] use VMD to decompose vibration signals into band-limited intrinsic mode functions (BLIMF), extract high-dimensional feature vectors using a high-dimensional common space pattern filter, and perform fault diagnosis using a random forest classifier. These methods achieve high-precision fault diagnosis by extracting more features or using more advanced classification algorithms. However, the complexity of the algorithms is gradually increasing. This requires more storage space, more computational resources, and more computation time, leading to an increase in hardware setup and operating costs.

M. Alonso-González and colleagues proposed a new approach for bearing fault diagnosis using envelope analysis and machine learning methods in 2023 [3]. This method aims to detect bearing faults with minimal observational data and features, achieving high diagnostic accuracy while reducing computational complexity. The process achieved high accuracy by combining frequency-domain vibration analysis with envelope analysis and leveraging the overlap of fault harmonics and characteristic frequencies. The Kernel

Naive Bayes model achieved an accuracy of 94.4%, while the Decision Tree (Fine Tree) and KNN (Fine KNN) models achieved a perfect accuracy of 100% [3]. This demonstrates that frequency domain vibration analysis, especially when using envelope analysis, is the optimal technology for detecting bearing faults. However, it is noted that this method cannot diagnose faults related to the ball, as the harmonics of rolling element faults do not overlap with characteristic frequencies. As a result, the technique achieves a three-class fault diagnosis for healthy status, inner race faults, and outer race faults.

Considering the above facts, this paper proposes a bearing fault diagnosis method based on vibration envelope spectrum features. Only the frequency and intensity (fai) of the fault characteristic peaks in the envelope spectrum are used as features, thereby reducing the variety of features. Meanwhile, the simple and efficient Naive Bayes algorithm is employed as the classifier to reduce the fault recognition time, ensuring accuracy while lowering algorithm complexity. In this study, evaluation is conducted using bearing fault data from both the CWRU dataset and the MFPT dataset. Firstly, the vibration signals of the bearings are demodulated using the Hilbert demodulation method to obtain the envelope spectrum. Next, multiple peaks and their frequencies are extracted from the envelope spectrum as fault features. Finally, a simple and efficient Naive Bayes classifier is utilized to classify the fault features and obtain diagnostic results.

2. Diagnosis Mechanism and Frequency Characteristics of Bearing Faults

Rolling bearings generally consist of inner rings, outer rings, balls, and retainers. During the operation of mechanical equipment, assembly errors, component failures of inner and outer ring balls, and localized deterioration can all lead to vibrations in the bearings.

The failure modes of rolling bearings can be classified into two categories: surface damage and local wear. The latter is a progressive failure, which is far less harmful than surface damage. Therefore, the focus of bearing failure diagnosis is on surface damage. The types of surface damage failure of rolling bearings mainly include outer race fault (ORF), inner race fault (IRF), and ball fault (BF).

Excluding the influence of structural and environmental factors, there are two main reasons for generating vibration in rolling bearings. The first is due to the high-frequency inherent vibration frequency caused by the elastic factor of the bearing itself [20]. The second is due to faults or damage inherent in the bearing components, manifested as impact vibration, with the frequency referred to as the bearing's intrinsic frequency [21]. It should be noted that the first form of vibration will inevitably occur during the bearing operation. In contrast, the second form of vibration only appears after a fault occurs, with each fault exhibiting different vibration characteristics.

The actual vibration is a nonlinear superposition of vibrations from the bearing and surrounding components, making the vibration characteristics much more complex than the analysis above. Electromagnetic interference from sensors and measurement circuits in the signal acquisition system can also affect the measured vibration signal, resulting from the complex interaction of multiple factors. Figure 1a–d shows vibration signals of different operating states for a fault diameter of 0.007 inches under 0 hp at a speed of 1797 rpm in the CWRU Dataset.

From Figure 1a–d, it can be seen that the vibration signal of the rolling bearing exhibits periodic variations and significant non-stationary characteristics. In the normal state, the bearing mainly shows a combination of inherent and mechanical system vibration, with small signal amplitudes and a characteristic of periodic decay. When a fault occurs in the bearing, the rolling elements generate impact excitation as they pass through the defective area, resulting in distinct impact modulation characteristics in the vibration signal, with the interval between impacts being related to the type of fault. Furthermore, the peak values of vibration signals for different fault types vary due to differences in the energy of impact excitation and the paths through which the energy reaches the sensor. As a result, the vibration characteristics produced at the sensor location are also different.

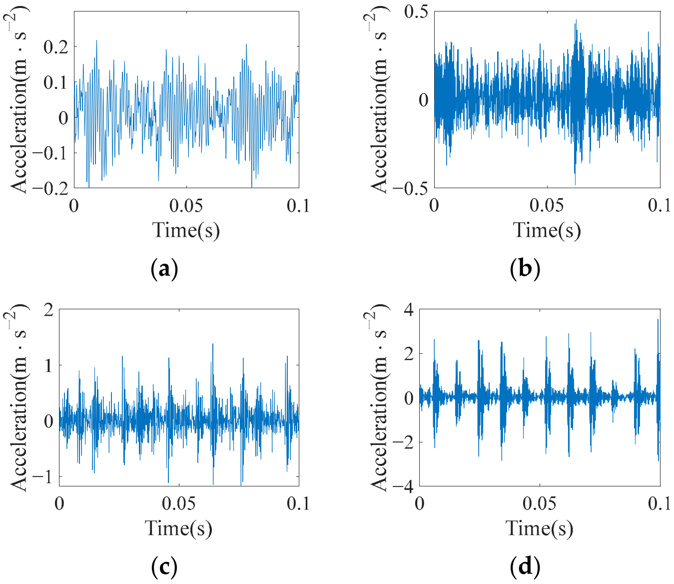

Figure 1. Vibration signals of (**a**) healthy (H), (**b**) ball fault (BF), (**c**) inner race fault (IRF), and (**d**) outer race fault (ORF).

Figure 1a–d illustrates vibration signals from different conditions. It can be observed that the pulse nature of the ball fault signal in Figure 1b is lower compared to other faults and resembles the signal of the healthy state depicted in Figure 1a. Although the amplitudes of the inner race fault signal in Figure 1c and the outer race fault signal in Figure 1d are higher than that of the healthy state, these two signals are similar. This complicates direct fault diagnosis through vibration signal analysis.

3. Method

In this work, vibration signals were obtained from both healthy bearings and bearings with different faults. By utilizing vibration analysis techniques, the fault classification of rolling bearings was achieved. The schematic flowchart of this method is shown in Figure 2.

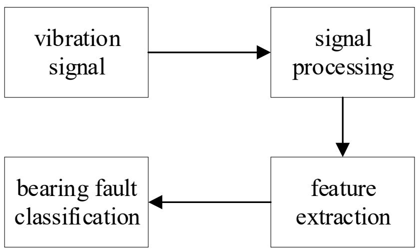

Figure 2. Flowchart of the proposed bearing fault detection method.

3.1. Signal Processing

In vibration signal processing, in addition to directly extracting the instantaneous amplitude, phase, and frequency of the vibration signal, the Hilbert transform can also demodulate the signal to obtain information about the interference and distortion of the signal's instantaneous attributes. Moreover, it can indicate the changes in frequency amplitude over time and extract some time–frequency characteristics that cannot be obtained using other methods [22].

When a bearing is faulty, the vibration signal spectrum often contains a lot of low-frequency noise interference. Through demodulation, the fault characteristic components modulated at high frequencies are demodulated to low frequencies, reducing low-frequency interference and improving the signal-to-noise ratio. In this work, the Hilbert transform is used to implement envelope demodulation of the signal, obtaining the envelope signal after filtering. The envelope signal retains the oscillating parts of the original signal and includes harmonics at the fault frequency.

The principal steps are as follows:

Step 1: Perform the Hilbert transform on the vibration signal $y(t)$:

$$\begin{aligned} \hat{y}(t) &= \frac{1}{\pi}\int_{-\infty}^{a} \frac{y(\tau)}{t-\tau} d\tau \\ &= \frac{1}{\pi}\int_{-\infty}^{a} \frac{y(t-\tau)}{\tau} d\tau = y(t) \times \frac{1}{\pi t} \end{aligned} \tag{1}$$

Here, $\hat{y}(t)$ is the envelope-demodulated signal obtained through convolution integration, and $1/\pi t$ is the impulse response of the convolution integration.

Step 2: Construct the analytic signal $s(t)$ of $y(t)$:

$$s(t) = y(t) + j\hat{y}(t) \tag{2}$$

Here, $j\hat{y}(t)$ is the imaginary part of the analytic signal.

Step 3: The envelope signal $Y(t)$ of the Hilbert transform of the signal $y(t)$:

$$Y(t) = \sqrt{\left[y(t)\right]^2 + \left[\hat{y}(t)\right]^2} \tag{3}$$

Step 4: After filtering the signal $Y(t)$ and performing a fast Fourier transform (FFT), the envelope spectrum of the original signal $y(t)$ can be obtained, from which characteristic information can be extracted.

Figure 3a–d shows the envelope spectra of vibration signals in different operating states with a speed of 1797 rpm, a fault diameter of 0.007 inches, and 0 hp in the CWRU Dataset. It can be observed from Figure 3a–d that there are significant differences in the peak values and corresponding frequencies of the envelope spectra for different operating states.

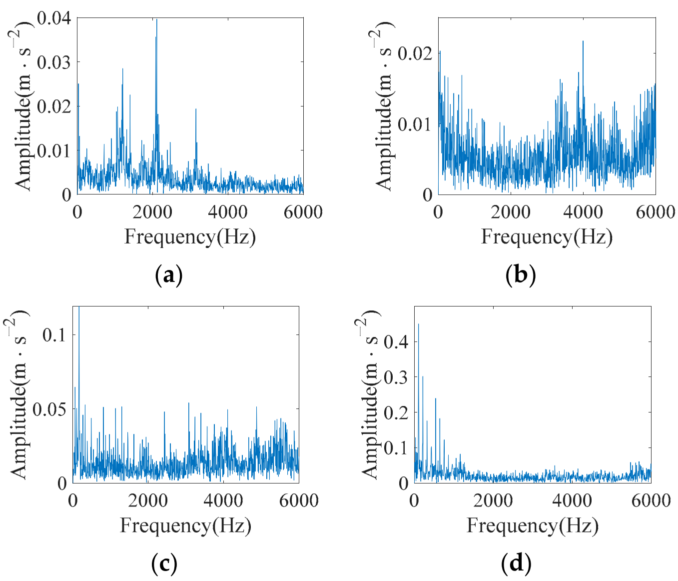

Figure 3. Envelope spectrum of the vibration signal of (**a**) H, (**b**) BF, (**c**) IRF, and (**d**) ORF.

3.2. Feature Extraction

Feature selection is an essential task in any classification problem because the performance of a classification model depends on the appropriate selection of features. Impact vibrations caused by faults typically form characteristic peaks on the envelope spectrum, and the intensity and corresponding frequencies of these peaks reflect the fault type and severity. The intensity of a feature peak refers to the peak value of the envelope spectrum, while the frequency of a feature peak corresponds to the frequency at which the peak value occurs in the envelope spectrum. Both the intensity and frequency of feature peaks can be obtained simultaneously.

Compared with widely used feature indicators in mechanical fault diagnosis, including mean value (mea), variance (var), kurtosis (kur), skewness (ske), and root mean square (rms). Using the CWRU and MFPT datasets of bearing faults, we evaluate fault diagnosis with different indicators as fault features using the Naive Bayes classifier.

Figure 4 presents the accuracy of fault diagnosis using different indicators as fault features across two datasets. In the CWRU dataset, the accuracy of the var, kur, rms, and fai feature indicators can all reach 90%, with fai achieving the highest accuracy at 99.6%. In the MFPT dataset, only the kur and fai feature indicators achieve 90% accuracy, with both reaching a high accuracy of 100.0%. Considering the diagnostic accuracy across both datasets, fai emerges as the most effective fault feature indicator.

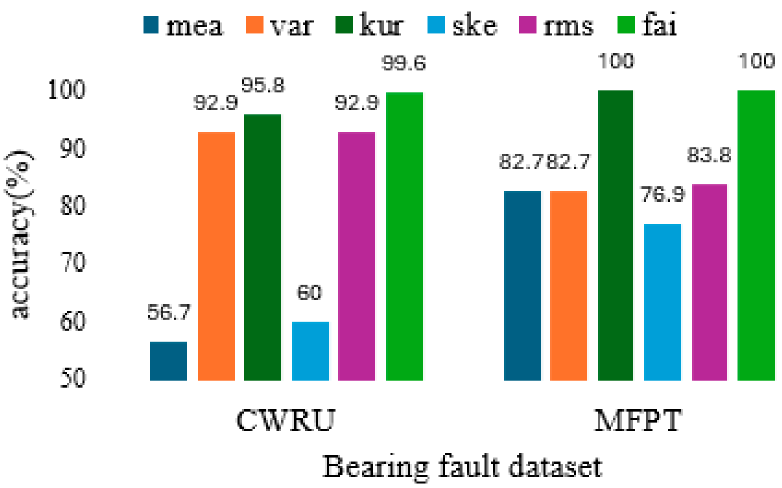

Figure 4. Classification accuracy of different feature indicators.

In this study, traversing the global envelope spectrum plot to identify multiple characteristic peaks would significantly increase the computational workload. Through calculation, the characteristic frequencies of faults in the ball, outer race, and inner race were determined to be 70.58, 107.36, and 162.19 Hz, respectively. Therefore, this study chose the envelope spectrum plot up to 200 Hz as the target for searching for fault characteristics. Four peak values and their corresponding frequencies extracted from the envelope spectrum are considered fault features, as shown in Figure 5a–d, arranged in ascending order of frequency. This feature extraction approach has a much lower algorithmic complexity than standard methods such as wavelet packet transform, principal component analysis, singular value decomposition, etc.

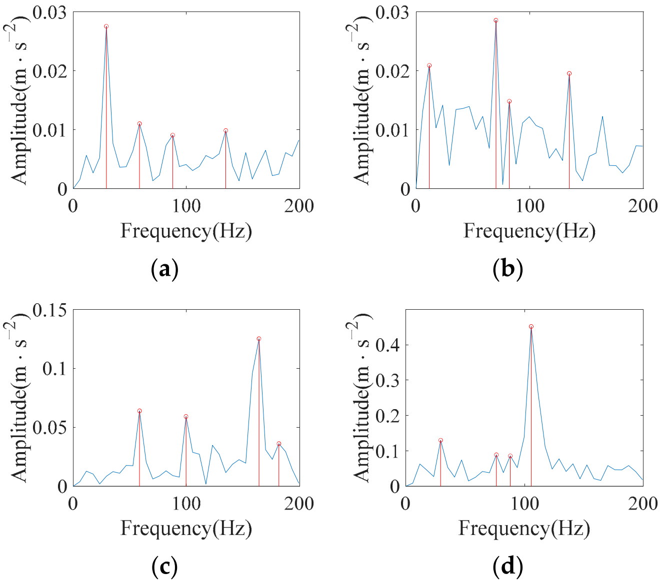

Figure 5. Peak extraction from envelope spectrum plots of (**a**) H, (**b**) BF, (**c**) IRF, and (**d**) ORF.

3.3. Naive Bayes Classifier

The Naive Bayes method is a classification approach based on Bayes' theorem and the assumption of conditional independence. It has good physical interpretability, and the diagnostic model is easy to implement. Compared to other classification algorithms, the Naive Bayes classifier is simple, robust to noise, has high parameter stability, strong overfitting handling capabilities, and boasts high learning and diagnostic efficiency. It requires very little storage space and has low computational cost [23]. By using it for fault diagnosis, the algorithm's complexity can be effectively reduced, diagnostic speed can be increased, the timeliness of real-time industrial bearing fault diagnosis can be enhanced, and hardware setup and operating costs can be minimized.

The Naive Bayes classifier assumes that the feature variables are conditionally independent given the class and each feature variable. Y_i is only related to the class variable C. Let $U = \{Y_1, Y_2, \cdots, Y_n, C\}$ be a finite set of discrete random variables, where $Y_1, Y_2, \cdots, Y_n$ represent the fault feature variables, y_i denotes the value of the fault feature Y_i, and the fault type C takes values from $\{c_1, c_2, \ldots, c_m\}$.

A faulty bearing sample $X = \{y_1, y_2, \ldots, y_n\}$, where $\{y_1, y_2, \ldots, y_n\}$ are the fault feature values. According to Bayes' theorem, the probability that this sample belongs to the fault class c_t is

$$p(c_t|y_1, y_2, \cdots, y_n) = \frac{p(y_1, y_2, \cdots, y_n|c_t)p(c_t)}{p(y_1, y_2, \cdots, y_n)} \tag{4}$$

Here, $p(c_t|y_1, y_2, \cdots, y_n)$ represents the posterior probability of predicting fault class c_t, $p(y_1, y_2, \cdots, y_n|c_t)$ is the conditional probability of having fault feature values $\{y_1, y_2, \ldots, y_n\}$ given fault class c_t, $p(c_t)$ is the prior probability of fault class c_t, and $p(y_1, y_2, \cdots, y_n)$ is the prior probability of fault feature values. The posterior probability reflects the impact of sample data on fault class c_t.

Since $p(y_1, y_2, \cdots, y_n)$ is constant for all fault classes, when $p(y_1, y_2, \cdots, y_n|c_t)p(c_t)$ is maximized, $p(c_t|y_1, y_2, \cdots, y_n)$ is maximized. The prior probability is

$$p(c_t) = \frac{N_{c_t}}{N} \tag{5}$$

where $t = 1, 2, \cdots, m$; N is the total number of training samples for bearing faults. N_{c_t} is the number of samples in the training set belonging to the fault class c_t.

On the premise of mutual independence among various fault characteristic values $y_1, y_2, \ldots, y_n$, the conditional probability is defined as

$$p(y_1, y_2, \cdots, y_n | c_t) = \prod_{i=1}^{n} p(y_i \mid c_t) \tag{6}$$

Here, $p(y_i \mid c_t)$ represents the conditional probability of fault characteristic value y_i under fault class c_t, which can be calculated from the training samples as

$$p(y_i \mid c_t) = \frac{N_{c_t}^{y_i}}{N_{c_t}} \tag{7}$$

Here, $N_{c_t}^{y_i}$ represents the number of samples in the training dataset where fault class c_t and fault characteristic value y_i coccur. If $N_{c_t}^{y_i} = 0$, then the probability is

$$p(y_i \mid c_t) = \frac{1/N}{N_{c_t} + N_{y_i}/N} \tag{8}$$

The probability $p(c_t|Y)$ that a fault sample belongs to a particular fault class c_i within fault type C can be obtained through Equations (4) to (5). If the probability of belonging to a certain fault class is maximum, then the bearing fault sample is classified into this particular bearing fault class.

4. Experimental Results and Analysis

The performance of this method was evaluated on the CWRU dataset [24] and the MFPT dataset [25].

4.1. Experimental Datasets

CWRU Dataset:

The CWRU dataset from Case Western Reserve University is a standard dataset for bearing fault diagnosis. The data was collected using a bearing vibration test rig, which includes a 2-horsepower motor, torque sensor/encoder, power meter, and electronic control equipment. Single-point damage faults were introduced on the outer race, inner race, and balls of the bearing through electrical discharge machining. The damage diameters are 0.007, 0.014, and 0.021 inches, respectively. Accelerometer sensors were installed on both the fan end (FE) and the drive end (DE) to collect vibration signal data. The sampling frequency for FE was 12 kHz, while for DE, it was 12 kHz and 48 kHz.

The experimental data selected for this experiment were sampled at a frequency of 12 kHz, with a fault diameter of 0.007 inches, a load range of 0 to 3 hp, and selected bearing conditions of H, BF, IRF, and ORF located at the 6 o'clock position. The CWRU dataset underwent sliding window processing, with a window size of 2048 and a step size of 400, resulting in approximately 4 $\times$ 299 samples.

MFPT Dataset:

The MFPT dataset comes from the public bearing dataset of the Mechanical Failure Prevention Technology Society. This dataset contains vibration signals under different operating conditions, including inner race faults, outer race faults, and normal conditions. Vibration data for normal conditions was collected using a test rig with NICE bearings at a 270 lb load and a sampling rate of 97,656 Hz, with a sampling time of 6 s. Seven datasets for outer race faults were collected, with load variations of 25, 50, 100, 150, 200, 250, and 300 lbs, at a sampling rate of 48,828 Hz and a sampling time of 3 s. Seven datasets for inner race faults were collected with load variations of 0, 50, 100, 150, 200, 250, and 300 lbs, at a sampling rate of 48,848 Hz and a sampling time of 3 s.

The experimental data selected for this experiment are as follows: since the vibration signals of bearings in a healthy state are generally smooth and less affected by load, the distribution of vibration signal data collected under different loads can be considered approximately equal. In the experimental design, all healthy state samples are selected under 270 lb with a sampling rate of 97,656 Hz. Vibration data for outer race fault and inner race fault are generated with a sampling rate of 48,828 Hz and loads of 150 lb, 200 lb, 250 lb, and 300 lb, respectively, for 3 s, forming four datasets. The MFPT vibration data was processed using a sliding window of 2048 steps with a stride of 400, resulting in approximately 3×362 samples.

We utilized 80% of the samples as the training set to train the model and the remaining 20% as the test set to validate the model's performance.

4.2. Evaluation Criteria

The confusion matrix is a tool used to evaluate the performance of a classification model, helping to understand the types of errors that occur during prediction. It consists of four parts: true positives, true negatives, false positives, and false negatives.

The performance of fault diagnosis results is evaluated based on three statistical parameters, namely accuracy (Acc), sensitivity (Sen), and specificity (Spe) [12], which are calculated from the respective confusion matrices of each classification result.

$$Acc(\%) = \frac{TP + TN}{TP + TN + FP + FN} \times 100 \tag{9}$$

$$Sen(\%) = \frac{TP}{TP + FN} \times 100 \tag{10}$$

$$Spe(\%) = \frac{TN}{TN + FP} \times 100 \tag{11}$$

where true positive (TP) and true negative (TN) represent the number of cases correctly classified, while false positive (FP) and false negative (FN) represent the number of cases incorrectly classified.

4.3. Analysis of Experimental Results

The selected fault features are input into the Naive Bayes classifier for bearing fault classification, thus completing the entire process of bearing fault diagnosis.

4.3.1. Experimental Results on the CWRU Dataset

Figure 6a–d presents the confusion matrix of bearing faults in the CWRU dataset using the proposed method.

The performance of bearing fault classification is shown in Table 1, with the classification accuracy reaching 99.58% for the 1st hp and 100.00% for the other three sets. The average accuracy is 99.90%, the average sensitivity is 99.90%, and the average specificity is 99.97%.

Table 1. Evaluation of fault detection results in CWRU.

Dataset	Acc (%)	Sen (%)	Spe (%)
0 hp	100.00	100.00	100.00
1 hp	99.58	99.58	99.86
2 hp	100.00	100.00	100.00
3 hp	100.00	100.00	100.00
average	99.90	99.90	99.97

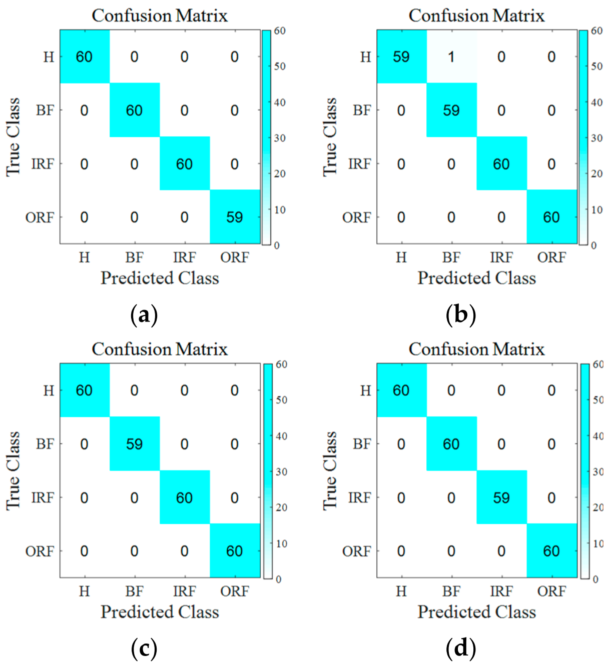

Figure 6. Confusion matrix of (**a**) 1 hp, (**b**) 2 hp, (**c**) 3 hp, and (**d**) 4 hp.

4.3.2. Experimental Results on MFPT Dataset

Figure 7a–d presents the confusion matrix of bearing faults in the MFPT Dataset using the proposed method.

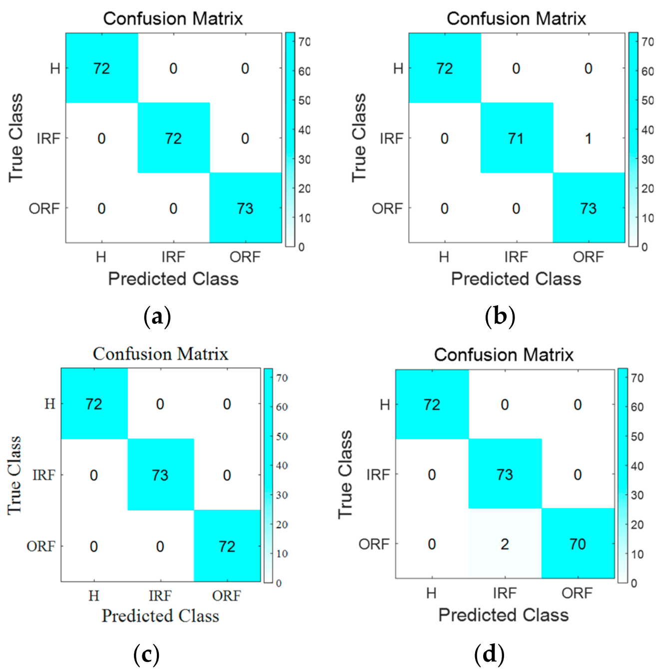

Figure 7. Confusion matrix of (**a**) 150 lb, (**b**) 200 lb, (**c**) 250 lb, and (**d**) 300 lb.

The performance of bearing fault classification is shown in Table 2. The average accuracy is 99.65%, the average sensitivity is 99.65%, and the average specificity is 99.89%.

Table 2. Evaluation of fault detection results in MFPT.

Dataset	Acc (%)	Sen (%)	Spe (%)
150 lb	100.00	100.00	100.00
200 lb	99.53	99.54	99.85
250 lb	100.00	100.00	100.00
300 lb	99.08	99.07	99.69
average	99.65	99.65	99.89

4.3.3. Comparison of Fault Diagnosis Using Different Classification Algorithms

To validate the simplicity and efficiency of the Naïve Bayes algorithm, accuracy and classification time were compared using CWRU 0 hp data and MFPT 150 lb bearing data against machine learning and deep learning algorithms, as shown in Figure 8. Fault diagnosis algorithms include random forest (RF), Support Vector Machine (SVM), convolutional neural network (CNN), convolutional neural network combined with Bidirectional LSTM (CNN-BiLSTM), Back Propagation (BP), and Long Short-Term Memory (LSTM).

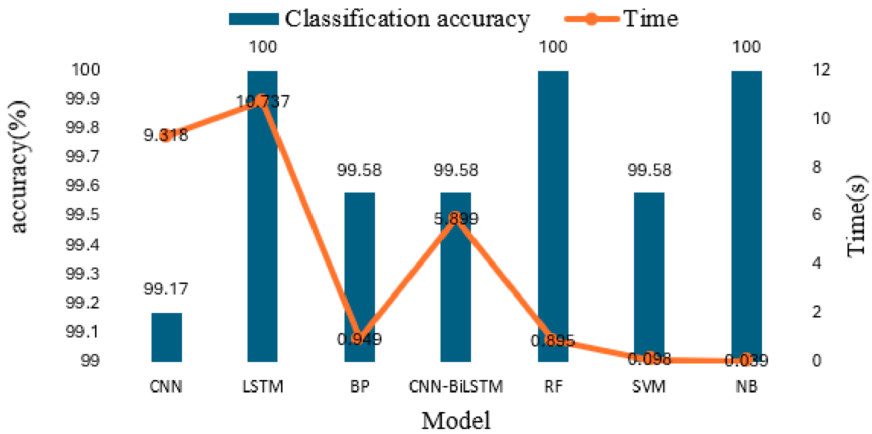

(**a**)

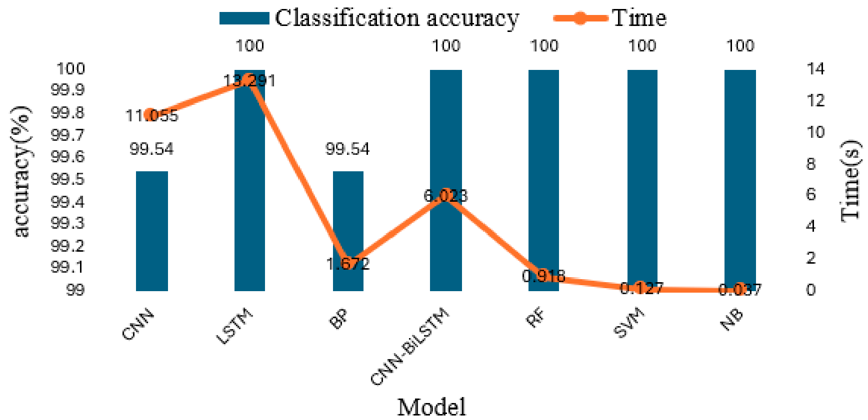

(**b**)

Figure 8. Diagnostic results of different classification algorithms on the (**a**) CWRU and (**b**) MFPT datasets.

From Figure 8, it can be observed that in the CWRU dataset, the accuracy of various classification algorithms reaches 99%, with LSTM, RF, and NB achieving a high accuracy of 100%. On the MFPT dataset, CNN and BP achieve an accuracy of 99.58%, while other algorithms achieve 100% accuracy. However, NB exhibits the shortest diagnostic time, significantly lower than all algorithms except SVM.

4.3.4. Analysis of Algorithmic Complexity of Fault Diagnosis Methods

The accuracy and algorithmic complexity of our experimental method were compared with literature published in the past 5 years that utilized the CWRU bearing database for fault recognition, as shown in Table 3. Due to the significantly higher algorithmic complexity of deep learning compared to machine learning, the algorithmic complexity of fault diagnosis methods based on deep learning is not further detailed here. Moreover, for facilitating algorithm complexity comparison, the sample size is uniformly set to N.

Table 3. Comparative study of fault diagnosis literature related to the current use of the CWRU.

Model	Year	Acc (%)	Algorithm Complexity
Laplacian Score, SVM [26]	2019	100.00	O(N(6144 + N))
Autocorrelation, RF [10]	2020	100.00	O(N(93 + 2018^2 + 250log(N)))
wavelet packet transform, RF [22]	2022	100.00	O(N(14,360 + 800Nlog(N)))
VMD, RF [27]	2022	99.67	O(N(4096 + 150log(N)))
envelope analysis, Fine KNN [3]	2023	100.00	O(N(3051))
this method		99.90	O(N(2280))

Table 3 shows that the accuracy of the diagnostic method proposed in this paper is similar to the accuracy of other algorithms. The algorithm complexity is close to reference [3] and much lower than other methods. Although the algorithm complexity in reference [3] is similar to the method proposed in this paper, it is limited to a three-class fault diagnosis for a healthy state, inner race fault, and outer race fault.

The results above indicate that the diagnostic method proposed in this paper has a high classification accuracy, significantly reduces algorithm complexity, improves classification efficiency, and is more suitable for industrial bearing fault diagnosis and maintenance.

5. Conclusions

To respond to the dramatic increase in algorithm complexity while achieving high accuracy in current fault diagnosis methods, this paper proposes a bearing fault diagnosis method based on vibration envelope spectrum features. This method utilizes the characteristic of periodic impact vibrations caused by bearing faults, which typically form periodic fault frequency peaks on the envelope spectrum. It extracts multiple peak values and their frequencies from the envelope spectrum as fault features and employs the algorithmically simple and efficient Naive Bayes classifier for fault classification. The algorithm's complexity in feature extraction and fault recognition aspects is reduced.

The following conclusion is drawn through theoretical analysis and experimental validation based on the CWRU dataset and the MFPT dataset. Compared to current bearing fault classification methods based on deep learning, data-driven techniques, etc., the proposed method significantly reduces algorithm complexity and computational hp while ensuring accuracy. It improves classification efficiency and is more suitable for real-time industrial bearing fault diagnosis. When dealing with complex datasets, such as variable-speed conditions, the classification performance of the proposed method in this paper may not be ideal. In such cases, methods that combine multiple classifiers can be used to further improve the results, which is the focus of our future work.

Author Contributions: Methodology, Y.C.; Software, Q.C.; Validation, Q.C.; Formal analysis, R.W.; Writing—original draft, Q.C.; Writing—review & editing, Y.C. and R.W. All authors have read and agreed to the published version of the manuscript.

Funding: This work was supported in part by the National Natural Science Foundations of China under Grant 62301086, in part by the Natural Science Foundation of Jiangsu Province under Grant BK20230627. This research was funded by the National Natural Science Foundations of China (62301086) and the Natural Science Foundation of Jiangsu Province (BK20230627). And The APC was funded by the Research on Anti-Multi-Target Interference Technology of Signal Processing with Space and Time Domain Deconvolution Arrays (6142109180206).

Institutional Review Board Statement: Not applicable.

Informed Consent Statement: Not applicable.

Data Availability Statement: Data is contained within the article.

Conflicts of Interest: The authors declare no conflict of interest.

References

1. Bankova, A. Investigation of the Qualitative Dependence between the Character of Wear and the Mutual Location of Wearing Supports. In Proceedings of the 2022 International Conference on Communications, Information, Electronic and Energy Systems (CIEES), Veliko Tarnovo, Bulgaria, 24–26 November 2022; pp. 1–4. [CrossRef]
2. Cui, L.L.; Jin, Z.; Huang, J.F.; Wang, H.Q. Fault Severity Classification and Size Estimation for Ball Bearings Based on Vibration Mechanism. *IEEE Access* **2019**, *7*, 56107–56116. [CrossRef]
3. Alonso-González, M.; Díaz, V.G.; Pérez, B.L.; G-Bustelo, B.C.P.; Anzola, J.P. Bearing Fault Diagnosis With Envelope Analysis and Machine Learning Approaches Using CWRU Dataset. *IEEE Access* **2023**, *11*, 57796–57805. [CrossRef]
4. Bao, W.J.; Tu, X.T.; Hu, Y.; Li, F.C. Envelope Spectrum L-Kurtosis and Its Application for Fault Detection of Rolling Element Bearings. *IEEE Trans. Instrum. Meas.* **2020**, *69*, 1993–2002. [CrossRef]
5. Nguyen, H.N.; Kim, J.; Kim, J.M. Optimal Sub-Band Analysis Based on the Envelope Power Spectrum for Effective Fault Detection in Bearing under Variable, Low Speeds. *Sensors* **2018**, *18*, 1389. [CrossRef]
6. Fan, W.; Zhou, Q.; Li, J.; Zhu, Z.K. A Wavelet-Based Statistical Approach for Monitoring and Diagnosis of Compound Faults With Application to Rolling Bearings. *IEEE Trans. Autom. Sci. Eng.* **2018**, *15*, 1563–1572. [CrossRef]
7. Zhang, X.; Wan, S.T.; He, Y.L.; Wang, X.L.; Dou, L.J. Bearing Fault Diagnosis Based on Iterative 1.5-Dimensional Spectral Kurtosis. *IEEE Access* **2020**, *8*, 174233–174243. [CrossRef]
8. Abdelkader, R.; Kaddour, A.; Derouiche, Z. Enhancement of rolling bearing fault diagnosis based on improvement of empirical mode decomposition denoising method. *Int. J. Adv. Manuf. Technol.* **2018**, *97*, 3099–3117. [CrossRef]
9. Wang, X.H.; Sui, G.Z.; Xiang, J.W.; Wang, G.B.; Huo, Z.Q.; Huang, Z. Multi-Domain Extreme Learning Machine for Bearing Failure Detection Based on Variational Modal Decomposition and Approximate Cyclic Correntropy. *IEEE Access* **2020**, *8*, 197711–197729. [CrossRef]
10. Roy, S.S.; Dey, S.; Chatterjee, S. Autocorrelation Aided Random Forest Classifier-Based Bearing Fault Detection Framework. *IEEE Sens. J.* **2020**, *20*, 10792–10800. [CrossRef]
11. Huang, Z.L.; Lei, Z.H.; Wen, G.R.; Huang, X.; Zhou, H.X.; Yan, R.Q.; Chen, X.F. A Multisource Dense Adaptation Adversarial Network for Fault Diagnosis of Machinery. *IEEE Trans. Ind. Electron.* **2022**, *69*, 6298–6307. [CrossRef]
12. Islam, M.M.M.; Kim, J.; Khan, S.A.; Kim, J.M. Reliable bearing fault diagnosis using Bayesian inference-based multi-class support vector machines. *J. Acoust. Soc. Am.* **2017**, *141*, EL89–EL95. [CrossRef] [PubMed]
13. Liu, J.; Zio, E. Integration of feature vector selection and support vector machine for classification of imbalanced data. *Appl. Soft Comput.* **2019**, *75*, 702–711. [CrossRef]
14. Khodja, A.Y.; Guersi, N.; Saadi, M.N.; Boutasseta, N. Rolling element bearing fault diagnosis for rotating machinery using vibration spectrum imaging and convolutional neural networks. *Int. J. Adv. Manuf. Technol.* **2020**, *106*, 1737–1751. [CrossRef]
15. Yang, B.; Fan, F.C.; Ni, R.R.; Wang, H.; Jafaripournimchahi, A.; Hu, H.Y. A multi-task learning network with a collision-aware graph transformer for traffic-agents trajectory prediction. *IEEE Trans. Intell. Transp. Syst.* **2024**, *25*, 6677–6690. [CrossRef]
16. Hoang, D.T.; Kang, H.J. A survey on Deep Learning based bearing fault diagnosis. *Neurocomputing* **2019**, *335*, 327–335. [CrossRef]
17. Encalada-Dávila, A.; Moyón, L.; Tutivén, C.; Puruncajas, B.; Vidal, Y. Early Fault Detection in the Main Bearing of Wind Turbines Based on Gated Recurrent Unit (GRU) Neural Networks and SCADA Data. *IEEE/ASME Trans. Mechatron.* **2022**, *27*, 5583–5593. [CrossRef]
18. Kaya, Y.; Kuncan, F.; Ertunç, H.M. A new automatic bearing fault size diagnosis using time-frequency images of CWT and deep transfer learning methods. *Turkish J. Electr. Eng. Comput. Sci.* **2022**, *30*, 1851–1867. [CrossRef]
19. Li, Z.L.; Lv, Y.; Yuan, R.; Zhang, Q.X. An Intelligent Fault Diagnosis Method of Rolling Bearings via Variational Mode Decomposition and Common Spatial Pattern-Based Feature Extraction. *IEEE Sens. J.* **2022**, *22*, 15169–15177. [CrossRef]

20. Su, W.S.; Wang, F.T.; Zhu, H.; Zhang, Z.X.; Guo, Z.G. Rolling element bearing faults diagnosis based on optimal Morlet wavelet filter and autocorrelation enhancement. *Mech. Syst. Signal Process.* **2010**, *24*, 1458–1472. [CrossRef]
21. Yang, X.Y.; Jing, S.X.; Luo, Z.P. Early Fault Diagnosis of Rolling Bearings based on LMS and Fast-Kurtogram. *Noise Vib. Control* **2019**, *39*, 172–176.
22. Feldman, M. Hilbert transform in vibration analysis. *Mech. Syst. Signal Process* **2011**, *25*, 735–802. [CrossRef]
23. Liu, R.; Yang, B.; Zio, E.; Chen, X. Artificial intelligence for fault diagnosis of rotating machinery: A review. *Mech. Syst. Signal Process.* **2018**, *108*, 33–47. [CrossRef]
24. Case Western Reserve University Bearing Data Center. Available online: https://engineering.case.edu/bearingdatacenter/download-data-file (accessed on 5 June 2024).
25. A Quick Introduction to Bearing Envelope Analysis, MFPT Data. Available online: https://www.mfpt.org/fault-data-sets (accessed on 6 June 2024).
26. Huo, Z.Q.; Zhang, Y.; Shu, L.; Gallimore, M. A New Bearing Fault Diagnosis Method Based on Fine-to-Coarse Multiscale Permutation Entropy, Laplacian Score and SVM. *IEEE Access* **2019**, *7*, 17050–17066. [CrossRef]
27. Han, T.; Gong, J.C.; Yang, X.Q.; An, L.Z. Fault Diagnosis of Rolling Bearings Using Dual-Tree Complex Wavelet Packet Transform and Time-Shifted Multiscale Range Entropy. *IEEE Access* **2022**, *10*, 59308–59326. [CrossRef]